Appl. Phys. B 72, 137–149 (2001) / Digital Object Identifier (DOI) 10.1007/s003400000443

Applied Physics B
Lasers
and Optics

High-power picosecond LiB_3O_5 optical parametric oscillators tunable in the blue spectral range

B. Ruffing*, **A. Nebel****, **R. Wallenstein**

Fachbereich Physik, Universität Kaiserslautern, Postfach 3049, 67663 Kaiserslautern, Germany

Received: 2 February 2000/Revised version: 28 July 2000/Published online: 22 November 2000 –

Abstract. The paper reports on an experimental investigation and numerical analysis of noncritically and critically phasematched LiB_3O_5 (LBO) optical parametric oscillators (OPOs) synchronously pumped by the third harmonic of a cw diode-pumped mode-locked Nd:YVO_4 oscillator–amplifier system. The laser system generates 9.0 W of 355-nm mode-locked radiation with a pulse duration of 7.5 ps and a repetition rate of 84 MHz. The LBO OPO, synchronously pumped by the 355-nm pulses, generates a signal wave tunable in the blue spectral range 457–479 nm. With a power of up to 5.0 W at 462 nm and 1.7 W at 1535 nm the conversion efficiency is 74%. The OPO is characterized experimentally by measuring the output power (and its dependence on the pump power, the transmission of the output coupler and the resonator length) and the pulse properties (such as pulse duration and spectral width). Also the beam quality of the resonant and nonresonant waves is investigated. The measured results are compared with the predictions of a numerical analysis for Gaussian laser and OPO beams. In addition to the blue-signal output visible-red 629-nm radiation is generated by sum-frequency mixing of the 1.535-μm infrared idler wave with the residual 1.064-μm laser radiation. A power of 1.25 W of 1.535-μm idler radiation and 5.7 W of 1.064-μm laser light generated a red 629-nm output power of 2.25 W.

PACS: 42.65.Yj, 42.65.Re, 42.70.Mp

Optical parametric oscillators (OPOs) synchronously excited by powerful near-infrared mode-locked lasers are very efficient sources for widely tunable ultrashort light pulses. The operating range of such OPOs is determined by the optical properties of the used nonlinear crystal (such as the birefringence and the spectral transparency range) and by the wavelength of the pump radiation. Since the pump radiation is usually generated with mode-locked solid-state lasers, such as Ti:sapphire, Nd:YLF or Nd:YAG, the pump wavelength is in the near infrared. Therefore the wavelengths of the OPO signal and idler waves are in spectral regions of the near- and mid-infrared. For the generation of ultrashort laser pulses at shorter wavelengths the frequencies of the infrared laser and OPO waves have been up-converted by frequency doubling and sum-frequency mixing. Frequency doubling of the infrared radiation of a mode-locked Ti:sapphire laser (680–1100 nm), for example, provides visible and UV radiation in a range extending from 340 nm to 550 nm [1–4]. The spectral region between the second harmonic and the fundamental laser radiation (which is in the range 550–680 nm) could be covered either by frequency-doubling the output of an OPO (pumped by a Ti:sapphire laser) [5–11], or by exciting an OPO with frequency-doubled Ti:sapphire laser pulses [12]. As the output power of mode-locked Ti:sapphire lasers is typically 2 W, the power of the generated visible laser light is well below 1 W. The generation of higher output powers requires more powerful pump lasers. Such lasers are, for example, passively mode-locked diode-pumped Nd:YVO_4 lasers [13, 14]. In contrast to the Ti:sapphire laser, the operation of these lasers is restricted to a fixed wavelength, which is preferentially the 1.06-μm transition.

For the direct generation of visible OPO radiation, the wavelength of the pump radiation has to be in the visible or in the ultraviolet spectral range. Such radiation is generated efficiently by the second, third or fourth harmonic of neodymium lasers (Nd:YAG, Nd:YVO_4) which provide powerful radiation at 0.53 μm, 0.35 μm or 0.26 μm. Whereas OPOs excited by the second harmonic operate in the yellow and red spectral range, OPOs pumped by the third or fourth harmonic also cover the blue spectral range. This was demonstrated, for example, by an OPO of lithiumtriborate (LBO) which was excited by the third harmonic of a lamp-pumped Nd:YLF laser. This LBO OPO generated cw mode-locked laser light at wavelengths in the range 453–472 nm with average output powers of up to 275 mW [15].

The nonlinear material LBO has several advantageous properties for the nonlinear conversion of infrared laser radiation into the visible or ultraviolet. It is well suited, for example, to the generation of the second and third harmonic

**Present address:* Spectra-Physics GmbH, Siemensstr. 20, 64289 Darmstadt, Germany
**Corresponding author.
(Fax: +49/631-205-3906, E-mail: nebel@rhrk.uni-kl.de)

of neodymium lasers [26]. It is also the material of choice for synchonously pumped OPOs which are excited by the 355-nm third harmonic. This is because of its optical transparency range which extends to wavelengths as short as 160 nm [19]. Therefore no deleterious absorptions are expected even for high-power operation in the blue and ultraviolet. Another important advantage is the noncritical phasematching (NCPM) of 532-nm or 355-nm pumped OPOs. The NCPM avoids spatial walk-off between the incident and generated waves and thus optimizes the interaction length and angular acceptance. In addition, the temperature acceptance is small [21, 26], which results in a wide wavelength tuning of the signal and idler waves by changing the crystal's temperature. Changing, for example, the crystal's temperature in the range 105–180 °C, the wavelengths of the signal and idler waves of the 532-nm pumped OPO are tuned in the range 670–2583 nm. For the OPO excited by 355-nm UV radiation the corresponding region is 458–479 nm for a temperature change of 25–190 °C.

In this paper we report on an investigation of a high-power LBO OPO synchronously pumped by the third harmonic of a cw mode-locked Nd:YVO_4 oscillator–amplifier system. Whereas synchronously pumped LBO OPOs reported so far provided ps light pulses with an average output power at the 0.5-W level [16–18], the LBO OPO investigated in this paper exceeded this power level by an order of magnitude and generated, for example, a visible blue output of up to 5 W at 462 nm when pumped by 9 W of 355-nm radiation.

The experimental characterization of this powerful all-solid-state laser device included the optimization of the frequency tripling of the Nd:YVO_4 solid-state laser (with respect to output power, pulse duration and beam quality), a detailed investigation of the performance of the signal-resonant LBO OPO, which included the wavelength tunability, and the dependence of the output power and efficiency on the pump power and the transmission of the output coupling mirror. In addition, the dependence of the output power and of the pulse parameters (such as pulse duration and spectral width) on the length of the OPO cavity are investigated. The measured performance is compared with the results of a numerical analysis which is based on a split-step Fourier approach for Gaussian laser and OPO beams. Besides the signal-resonant OPO, also idler-resonant OPOs are investigated. The idler-resonant OPO configurations use noncritically or critically phasematched crystals with Brewster-cut or AR-coated facets.

1 Third-harmonic generation

The LBO OPOs described in this paper are excited by the third harmonic of a diode-pumped passively mode-locked Nd:YVO_4 oscillator–amplifier system. The 355-nm third harmonic is generated by sum-frequency mixing (SFM) the second harmonic and the fundamental of the Nd:YVO_4 laser system.

The Nd:YVO_4 oscillator, which is similar to systems previously reported [13, 24], is passively mode-locked by a high-finesse antiresonant Fabry–Pérot saturable absorber (AFPSA). When pumped by 12 W of 808-nm cw diode-laser radiation the oscillator provides an output of 4.5 W in a nearly diffraction-limited beam ($M^2 < 1.1$). The duration of the almost bandwidth-limited pulses is 10 ps, the repetition rate 84 MHz. The output of the oscillator is amplified in a three-stage amplifier. In the first (double-pass) amplifier stage the average power is increased to 12 W. The average powers behind the second and third amplifier are 20 W and 28 W, respectively. Since each amplifier is pumped by 24 W of 808-nm cw diode-laser radiation the total diode pump power amounts to 84 W. The output power of 28 W thus corresponds to an optical efficiency of 33%. Despite the thermal lensing in the Nd:YVO_4 amplifier crystals the output beam is close to the diffraction limit ($M^2 < 1.1$).

For second-harmonic generation (SHG) the Nd:YVO_4 laser output is passed through a 23-mm long LBO crystal, cut for noncritical ($\Phi = 0°$, $\Theta = 90°$) type-I (oo → e) temperature phasematching. The noncritical type-I phasematching has several advantages compared to critical type-II phasematching (used, for example, in KTP, oe → e), in particular if the second harmonic and the residual radiation of the fundamental are used for SFM. For type-I phasematching the fundamental light pulses propagate as an o-polarized wave. For type II, however, the fundamental pulses propagate partly as an extraordinary (e-) and partly as an ordinary (o-) polarized wave. Therefore, the phase and group velocities of both parts are different. Due to the walk-off, the o- and e-beams are in part spatially separated after propagating through the crystal. Those parts of the beams which still overlap are elliptically polarized. In addition the group velocity mismatch (GVM) distorts the temporal profile of the pulses. Type-I phasematching avoids these problems with the result that the temporal beam profile of the SHG laser pulses is not distorted by GVM, the spatial profile is not changed by walk-off effects and the polarization remains linear.

Noncritically phasematched SHG requires a crystal temperature of about 148.5 °C [20]. In the experiment the crystal is heated in an oven, whose temperature is controlled with an accuracy of 0.1 °C. The 28 W output of the oscillator–amplifier system is focused into the LBO crystal to a beam waist of 37 μm. The measured 532-nm output power is 22.4 W which corresponds to a conversion efficiency of 80%. The second-harmonic pulses are nearly transform-limited with a duration of 9 ps. The 532-nm laser beam is close to the diffraction limit ($M^2 < 1.2$).

The third harmonic (THG) is generated by SFM of the 1064-nm fundamental and the 532-nm second-harmonic laser pulses in LBO. For this SFM process critical type-I phasematching (oo → e) or type-II (oe → o) critical phasematching can be used. The characteristic data for the type-I and type-II conversion are compared in Table 1. Although the effective nonlinearities and the bandwidth acceptances are similar, the main differences are in the spatial walk-off and the angular acceptance. A high conversion and a nearly diffraction-limited beam (with a circular cross-section) requires a small walk-off and a large angular acceptance. For this reason the small walk-off of type-II phasematching is of advantage. This is confirmed by calculating the ratio of the parametric efficiency coefficients for type-I and type-II phasematching [30]. These calculations take into account the spatial and temporal walk-off as well as diffraction and dispersion. For the same values of the beam waist, pulse duration and crystal length the calculated value is 1.0 : 3.3 showing the higher potential of type-II phasematching. Additionally type-II phasematching provides an angular acceptance that is about three times larger, which should result in a superior spatial beam profile,

Table 1. Characteristic data for third-harmonic generation by sum-frequency mixing of the fundamental 1064-nm radiation with the 532-nm second harmonic in LBO using type-I or type-II phasematching. The data are based on the Sellmeier equations given in [19]

		Type I, oo-e, xy-plane	Type II, oe-o, yz-plane
Phasematching angle		$\Phi = 37.3°$; $\Theta = 90°$	$\Phi = 90°$; $\Theta = 42.7°$
Nonlinearity [19]	d_{eff}	0.9 pm/V	−0.8 pm/V
Spatial walk-off	ϱ	1.1°	−0.5°
Angular acceptance	$\Delta\Theta \cdot L$	0.5 mrad · cm	1.6 mrad · cm
Bandwidth acceptance	$\Delta\lambda \cdot L$	0.75 nm · cm	0.83 nm · cm
Group velocity mismatch	$\Delta v_{\text{gr}}^{-1}$		
1064 nm/355 nm		216 fs/mm	281 fs/mm
532 nm/355 nm		116 fs/mm	62 fs/mm

if the laser radiation is tightly focused into the LBO crystal. Moreover, for type-II phasematching the walk-off can in principle be compensated by tilting the direction of the e-polarized 532-nm beam with respect to the direction of the o-polarized 1064-nm laser beam by a small angle. This compensation is usually done by optimizing the efficiency of the output of the generated third harmonic if the experimental setup allows for such adjustments of the beam directions.

In the experiment a 20-mm long type-II LBO crystal ($\Phi = 90°$, $\Theta = 42.7°$) was used for SFM. The facets of the crystal were AR-coated for 1064 nm, 532 nm and 355 nm. As the temperature acceptance of the 20-mm long crystal is 2.9 °C the crystal temperature was stabilized in a simple way by a Peltier element at room temperature.

The fundamental and the frequency-doubled laser waves travel at different velocities in the SHG- as well as in the THG-crystal. This causes a time delay between the fundamental and the green laser pulses of 0.6 ps in the SHG- and 2.2 ps in the THG-crystal. To compensate this delay the beams are separated by the dichroic mirror M1 (see Fig. 1). The separated beams are collimated by the AR-coated lenses L1 and L2. The fundamental laser beam is delayed by a delay line of length ΔL and recombined with the second harmonic by the dichroic mirror M2. The spatial separation of both beams allows us to focus the fundamental and SH separately using the spherical lenses L3 and L4 into the LBO crystal, and

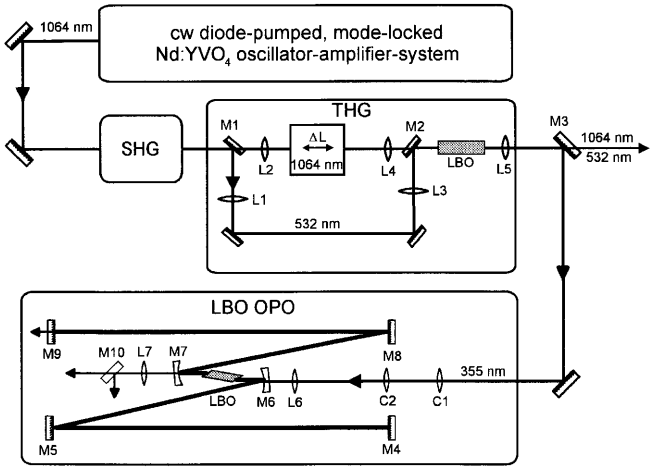

Fig. 1. Scheme of the experimental setup. For details see text

to optimize the beam directions in order to compensate for the spatial walk-off between the fundamental o-polarized and the frequency-doubled e-polarized wave. The third harmonic is collimated by lens L5 and separated by the dichroic mirror M3 from the fundamental and green laser radiation.

The efficiency of the SFM mainly depends on the temporal and spatial overlap of the light pulses, on the pulse powers of the fundamental and green radiation and on the power ratio. The temporal overlap is adjusted by changing ΔL in the delay line. The duration of the residual light pulses at the fundamental is 13 ps. These pulses are broadened compared to the 10-ps long laser pulses because of the saturation of the conversion in the SHG crystal. The pulse duration of the frequency-doubled green pulses was about 8 ps when the SHG conversion efficiency was reduced to about 45% in order to keep a certain amount of power in the residual infrared laser beam.

The spatial overlap depends on the confocal parameters and the position of the beam waists w_1 and w_2 of the infrared and green laser radiation, which can be changed by the focal lengths and the positions of the lenses L3 and L4. The efficiency of the THG was measured for different ratios of the beam waist w_1 of the fundamental and w_2 of the second harmonic (see Table 2). For a beam waist of 30 μm for both the fundamental and the green beam, an optimum conversion efficiency of 50% was measured. The corresponding average power in the 355-nm UV beam was 11.5 W, generated from 11.5 W at 1064 nm and 12.5 W at 532 nm, which adds up to a total input of 24.0 W. A small increase of w_1 from 30 μm to 40 μm reduces the efficiency only by a small amount to about 48%. A further increase of w_1 to 70 μm, however, reduces the efficiency to 39%. In contrast to w_1, only a slight increase of w_2 to 40 μm is required to reduce the efficiency to 42%. This efficiency is further reduced to only 21% for a w_2 waist of 70 μm. This experiment shows that the highest efficiency is achieved for beam waists of equal size. Whereas a small increase of w_1 reduces the efficiency by less than 10%, the efficiency is reduced considerably for larger values of w_2. The greater variation in THG efficiency with harmonic beam size compared with the fundamental beam size is given by the faster reduction of the spatial overlap caused by the different confocal parameters.

The infrared laser pulses used for SFM are partially depleted in power by the SHG and are thus broadened in time. An increase in efficiency could be expected by using nondepleted infrared laser pulses. For this reason a part of the fundamental beam was separated in front of the SHG

Table 2. Conversion efficiency for the third harmonic generated by sum-frequency mixing of the fundamental (1064 nm) with the second-harmonic (532-nm) laser radiation measured for different focussing conditions

Beam waist w_1 (1064 nm)	Beam waist w_2 (532 nm)	Efficiency
70 μm	30 μm	39%
40 μm	30 μm	48%
30 μm	30 μm	50%
30 μm	40 μm	42%
30 μm	70 μm	21%
70 μm	70 μm	39%

unit and then used for sum-frequency mixing with the green laser beam. In fact, this configuration provided a slightly higher internal conversion efficiency of 54% for the SFM process. However, the output power did not exceed the value of 11.5 W obtained in the first setup. This is because the total input power decreased. In the experiment 8.2 W was separated from the infrared laser beam for SFM. The residual infrared power of 19.8 W was focused for SHG into the LBO crystal. The generated power of 532-nm radiation was 14.0 W, which corresponds to an efficiency of 70%. With an input of 8.2 W of 1064-nm radiation and 14 W of 532-nm radiation the SFM generated 355-nm radiation with a power of 11.5 W. Obviously the improved temporal and spatial quality of the 1064-nm beam compensates for the somewhat lower total power input of 22.5 W.

During operation at the highest UV output power of 11.5 W a slow decrease of the power in time at a rate of about 5% per hour was observed. At a somewhat reduced UV power of 9 W the output remained more stable. For this reason a power of 9.0 W was used routinely to excite the synchronously pumped LBO OPO.

To determine the pulse duration of the 355-nm radiation an intensity autocorrelation measurement was not possible because there is no nonlinear material which provides phasematched SHG at this wavelength. The SHG is commonly used as a correlation signal. Instead a cross-correlation measurement was generated by difference-frequency mixing (DFM) of the 355-nm and the 532-nm radiation in a 20-mm long LBO crystal ($\Phi = 90°, \Theta = 42.7°$). Such a cross-correlation signal is shown in Fig. 2 as function of the time delay between the UV and 532-nm laser pulses.

The width at half-maximum of this DFM signal is 12.3 ps. The half-width was the same when measured with LBO crystals of different length L (20 mm, 15 mm or 6 mm). Dispersive effects and the bandwidth acceptances of the different crystals obviously do not influence the result of the cross-correlation measurement. To calculate the exact pulse duration by deconvolution of the cross-correlation signal the pulse shape of the 532-nm pulse has to be known precisely and the DFM has to be measured with the lowest efficiency. However, the pulse shape can not be extracted from an intensity autocorrelation and the efficiency of the DFM exceeded 5%. Therefore, the output of the DFM was numerically calculated as a function of the delay of the input pulses for a fixed duration of the green light pulses of 8 ps and different pulse durations of the UV pulses. The numerical algorithm used is similar to the algorithm described for an OPO [23], and takes Gaussian beams into account. The complex-valued, z-dependent spatial beam overlap factors taken from [22] are used in the nonlinear amplitude equations. In this case the maximum output power of the DFM is not obtained for the phasematching condition for plane waves ($\Delta k = 0$) but for a value of Δk of 130 m^{-1}. This value was calculated for identical beam waists of 30 μm. The half-widths of the DFM signal obtained using these calculations are shown in the insert of Fig. 2; they depend on the pulse duration of the UV pulses. As seen from this figure the measured half-width of 12.3 ps is obtained for a UV pulse duration of 7.5 ps. The shape of the measured DFM signal (solid curve) is in good agreement with the calculated line shape (dashed line).

The beam profile in the far field of the generated UV radiation is elliptical, with an ellipticity of 1.6. The short axis of the ellipse is directed along the phasematching plane of the crystal, the long axis is perpendicular to it. This ellipticity is in part due to the spatial walk-off. The spatial walk-off of 0.5° of the e-polarized green beam was, however, compensated by adjusting this beam in a slightly noncollinear direction to the fundamental beam. In this way the overlap of all three beams in the crystal is maximized. However, the angular acceptance of 0.8 mrad in the phasematching plane restricts spatially the phasematching in the crystal volume, and thus causes the elliptical shape of the beam profile. The UV beam is nearly diffraction-limited with M^2 values of less than 1.3 in both planes. In order to obtain a focus with a circular cross-section for an application such as, for example, the excitation of an OPO, the beam could be shaped by an appropriate cylindrical telescope.

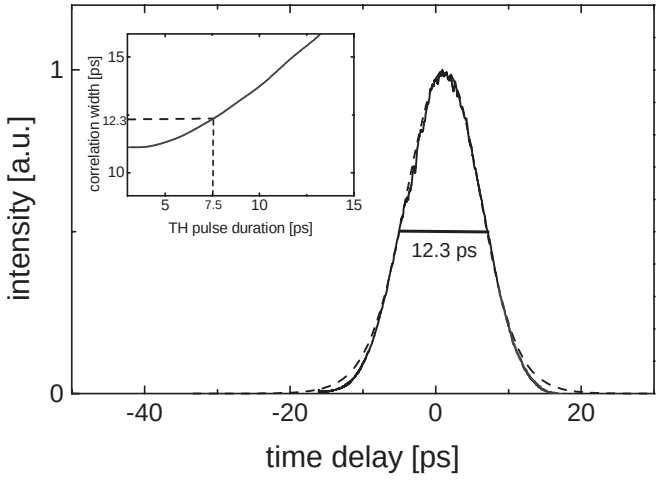

Fig. 2. Cross-correlation signal as a function of the time delay of the input pulses. *The dashed line* corresponds to the result of the numerical simulation for a 355-nm pulse duration of 7.5 ps. *The insert* shows the numerically calculated correlation width as a function of the pulse duration of the 355-nm pulses

2 Signal-resonant noncritically phasematched OPOs

The scheme of the signal-resonant noncritically phasematched OPO which is pumped by the 355-nm third harmonic of the Nd:YVO_4 oscillator–amplifier system is shown also in Fig. 1. The optical resonator is a folded, astigmatically compensated linear cavity which consists of four flat mirrors (M4, M5, M8 and M9) and two spherical mirrors (M6 and M7) with a radius of curvature of $r = -200$ mm. The mirrors M4–M8 are highly reflective ($R > 99.9\%$) for the blue-signal wave. In the experiment the transmission of the output coupling mirror M9 is varied in the range 2%–92%.

The 18-mm long LBO crystal is cut for noncritical type-II (e → oe) phasematching ($\Theta = 0°$, z-cut). Due to the noncritical phasematching the interaction length is not limited by spatial walk-off between the pump and the signal beam, and therefore the angular acceptance has its maximum value. The facets of the crystal are Brewster-cut to minimize the losses for the resonant o-polarized signal wave. On these facets the e-polarized pump and idler waves are partly reflected, however, which causes a loss of about 17% for each wave.

The pump beam is focused into the LBO crystal by the spherical lens L6 to a beam waist of 20–30 μm which is close to the calculated value of the waist of the TEM_{00} resonator mode of 30 μm at 460 nm. While the generated resonant signal wave is partly transmitted by the output coupler M9, the idler wave is transmitted by M7 and separated from residual pump radiation by the dichroic mirror M10.

Since the pump beam passes through the tilted mirror M6 and the Brewster-cut crystal facet the focus is astigmatic. This astigmatism (measured by the distance between the sagittal and tangential beam waist) can be changed by a cylindrical telescope placed in front of the focusing lens L6. The astigmatism influences the OPO efficiency and thus the depletion of the pump beam. Figure 3 shows the dependence of the pump depletion on the astigmatism of the pump beam. With a cylindrical telescope consisting of the lenses C1 and C2 the astigmatism is changed in the range of ±8 mm. Over the whole range the pump depletion exceeds 50%. It is interesting to note that for an astigmatism of ±8 mm the tangential focus plane is located at a distance of 1 mm behind the crystal's front surface while the sagittal plane is located in the crystal's center. If the astigmatism is reduced to zero (which corresponds to a beam waist of 21 × 21 μm) the pump depletion is increased to 78%. As seen from Fig. 3 a small astigmatism of up to ±3 mm hardly changes the pump depletion, and should thus be tolerable.

The powers of the generated signal and idler waves were measured as functions of the transmission of the output coupler (OC). The results obtained for a pump power of 9.0 W and for a 479-nm signal and 1371-nm idler wave are shown in Fig. 4. As seen from this figure a maximum OPO output is achieved with an OC transmission of 37%. With this OC the OPO generated a signal power of 3.4 W and an idler power of 0.65 W. With respect to the pump power inside the crystal (which is 6.4 W due to losses at lens L6, mirror M6 and the Brewster facet of the crystal) the total output of 4.05 W corresponds to an internal conversion efficiency of 75%. It is interesting to note that the OPO still generates a signal output of more than 2 W if operated with an OC transmission of 69%. The solid line in Fig. 4 represents the results of a numerical analysis [23, 24]. The calculated values are in good agreement with the measured data of most of the OC transmission

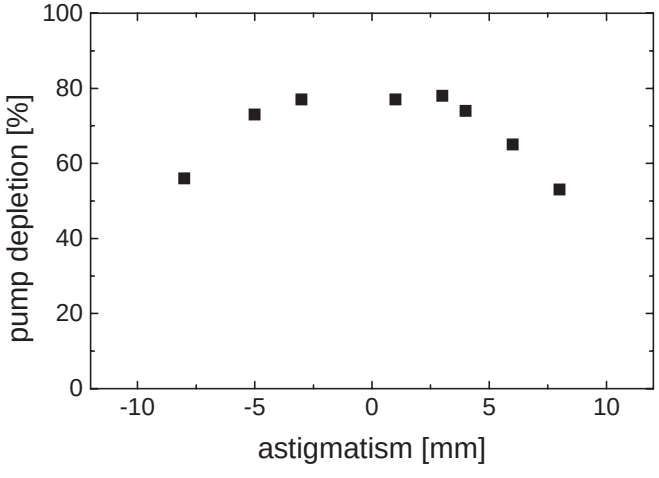

Fig. 3. Pump depletion as a function of the astigmatism (distance between the tangential and sagittal focus plane) of the pump radiation

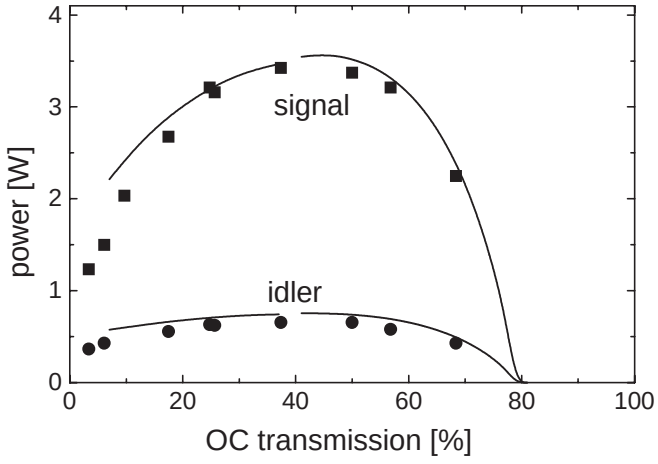

Fig. 4. Average power of the 479-nm signal and the 1371-nm idler wave as a function of the transmission of the output coupler. *The squares* are the measured values, *the solid lines* represent the data obtained by the numerical analysis. The power of the 355-nm pump radiation is 9 W

values. The numerical analysis indicated that for different OC transmissions the generation of a maximum output requires different resonator lengths. However, the output power is reduced by less than 4%, even if the change ΔL of the resonator length amounts to a substantial fraction of ΔL_{m}. ΔL_{m} is the maximum possible change of the resonator length, which maintains OPO operation. For example, using an OC transmission (T_{OC}) of 60%, 96% of the maximum output power is obtained for ΔL in the range $160\,\mu\mathrm{m} < \Delta L < 280\,\mu\mathrm{m}$. This is a considerable fraction of $\Delta L_{\mathrm{m}} = 250\,\mu\mathrm{m}$ (determined by the interval $125\,\mu\mathrm{m} < \Delta L < 375\,\mu\mathrm{m}$). For a T_{OC} of 40%, 96% of the optimum output is obtained within the wide range $180\,\mu\mathrm{m} < \Delta L < 335\,\mu\mathrm{m}$, which corresponds to 56% of $\Delta L_{\mathrm{m}} = 280\,\mu\mathrm{m}$ ($125\,\mu\mathrm{m} < \Delta L < 405\,\mu\mathrm{m}$).

The basic algorithms used for the numerical analysis are described in detail in [23, 24]. They considers the parametric gain, the group velocity mismatch (GVM) and the resonator properties such as resonator length and optical losses. The pump and the OPO waves are described by Gaussian beams with complex-valued spatial beam overlap factors, as described in detail in [22]. These overlap factors change with the propagation through the OPO crystal. As a result the model assumes three TEM_{00} beams with identical positions of the beam waist. This approximation is valid, if the nonlinear interaction does not significantly change the beam profile, which is true for noncritically phasematched OPOs, where, for example, the angular acceptance is sufficiently large and no spatial walk-off occurs. The algorithm of the numerical simulation is based on a split-step Fourier method which is similar to that reported in [23, 24].

As seen from Fig. 5 the measured pump power at the threshold increases from 0.5 W for $T_{\mathrm{OC}} = 3\%$ to 3.7 W for $T_{\mathrm{OC}} = 57\%$. This figure shows also the dependence of the signal power on the pump power present in the LBO crystal for different OC transmissions. In these measurements the OPO was operated at room temperature, the signal wavelength was 479 nm. The measurements show a strong increase of the slope efficiency with OC transmission. It is interesting to note that for a T_{OC} of 57% the slope still decreases from about 140% close to the threshold to about 70% for a pump power of 6.0 W. This indicates that even for such high T_{OC}, gain sat-

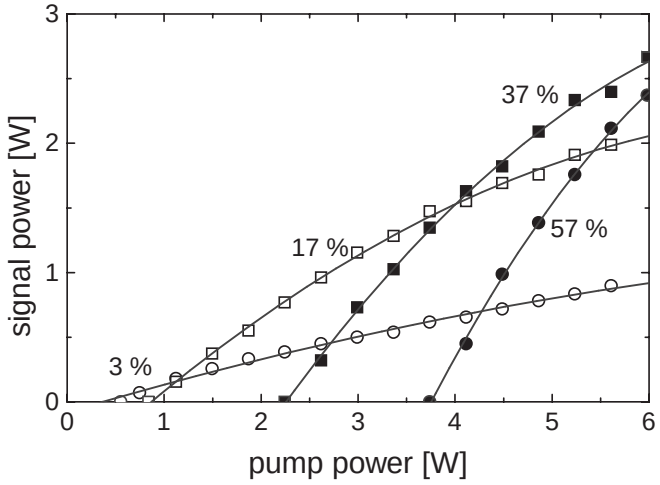

Fig. 5. Dependence of the power of the 479-nm signal radiation on the pump power measured for different OC transmissions

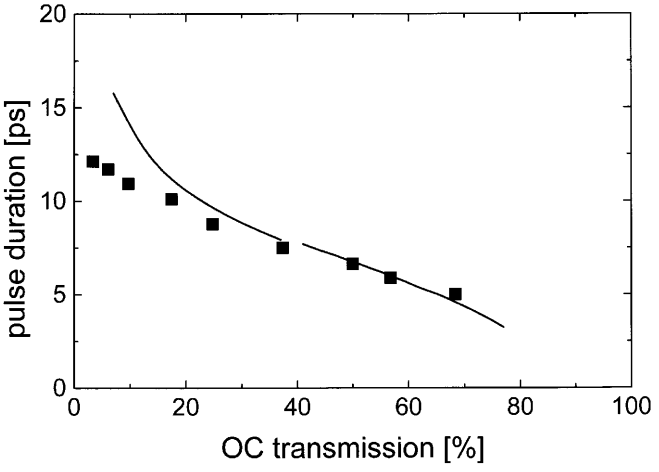

Fig. 7. Dependence of the duration of the 479-nm signal pulses on the OC transmission. *The squares* represent the measured data, *the solid line* represents the values provided by the numerical analysis. The 355-nm pump power is 9 W

uration (caused by pump depletion and reconversion of signal and idler into pump radiation) reduces the efficiency.

The pulse properties determined by an intensity autocorrelation and the corresponding pulse spectrum are shown in Fig. 6. These measurements were taken for an OC transmission of 37%. To calculate the pulse duration from the measured width of the intensity autocorrelation, the decorrelation factor, which is the ratio of the autocorrelation to the pulse width, has to be known. This factor strongly depends on the shape of the OPO pulses. Usually it is assumed that this shape is the same as that of the pump pulse. However, the shape of the OPO pulses changes if the nonlinear process is very efficient and if the resonator length is changed. Therefore, we used the measured spectral shape and numerically calculated the pulse duration and the decorrelation factor with respect to this spectrum. With a calculated factor of 0.72 the autocorrelation width of 10.4 ps shown in Fig. 6 corresponds to a pulse duration of 7.5 ps. The pulse spectrum was measured with a scanning Fabry–Pérot interferometer with a free spectral range of 300 GHz. With a spectral width of 71.4 GHz the time–bandwidth product is 0.54. The comparison with the numerically calculated value of 0.59 indicates that the pulses are almost bandwidth limited.

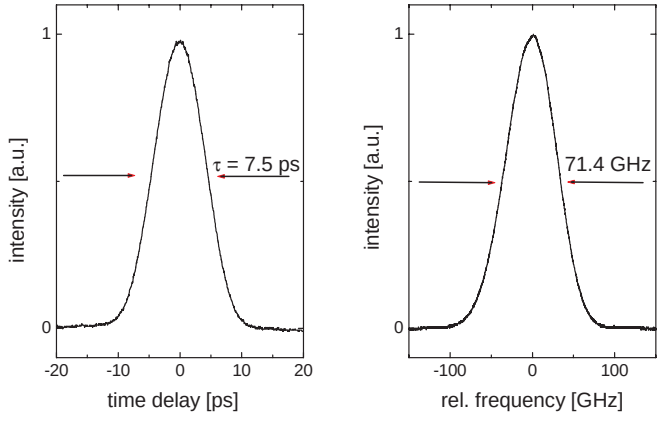

Fig. 6. Intensity autocorrelation and spectrum of the 479-nm OPO signal pulses for an OC transmission of 37%. The power of the 355-nm pump radiation is 9 W

The durations of the signal pulses vary with OC transmission (Fig. 7). The squares represent the pulse duration for the resonator length which provides a maximum output power. The pump power is 9.0 W. As seen from Fig. 7 the pulse duration decreases from 12 ps for $T_{OC} = 3\%$ to 5 ps for $T_{OC} = 69\%$. For $T_{OC} = 37\%$ the pulse duration is 7.5 ps. For this T_{OC} the OPO is operated 1.8 times above the threshold. In the numerical analysis the signal-pulse durations are determined from the calculated envelope of the signal pulses. The experimental pulse widths are obtained from autocorrelation measurements.

The wavelength of the OPO can be tuned by changing the temperature of the LBO crystal. In Fig. 8 the wavelengths of the signal and idler waves are shown as functions of the temperature of the LBO crystal. The squares represent the measured data. For a temperature change from 20 °C to 190 °C the wavelength of the signal radiation tunes from 479 nm to 458 nm. The corresponding wavelengths of the idler wave are 1360–1580 nm. The solid line represents the wavelengths

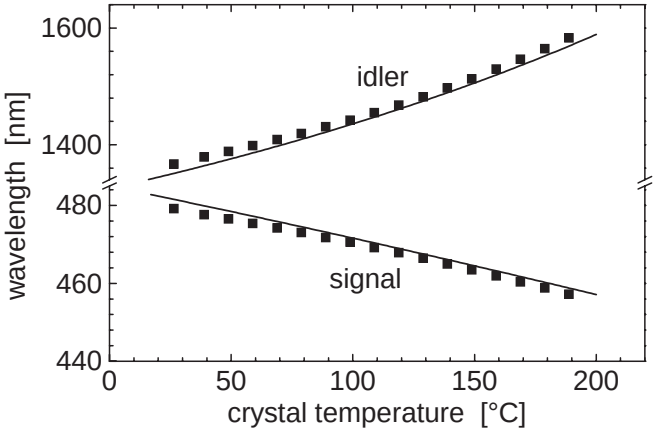

Fig. 8. Wavelength of the signal and idler radiation as a function of the temperature of the LBO crystal. *The squares* are the measured data, *the solid lines* are given by calculations based on the Sellmeier equations given in [22]

calculated from the Sellmeier equations which include the so-called improved temperature-dependent temperature coefficients [21]. The small differences between the measured data and the experimental values (which range for the signal wave from 0.9 nm to 2.1 nm) could result from a difference between the actual temperature in the crystal and the value displayed on the oven control unit, as well as from temperature gradients within the center of the crystal caused by light absorptions [29]. In addition it has to be considered that maximum efficiency is obtained for the phasematching condition $\Delta k = 0$ only if the interacting light fields are plane waves. For Gaussian beams, which are nearly confocally focused, maximum conversion efficiency is not obtained for perfect phasematching ($\Delta k = 0$) but for $\Delta k > 0$. This result was obtained analytically in the approximation of negligible pump depletion [25]. The numerical calculations, which assume beam waists of 30 μm, indicate also that for high conversion efficiencies (as high as 70%) the output is an optimum for $\Delta k > 0$. For the present experimental conditions a maximum output was in fact calculated for a phase mismatch of $\Delta k = 140\,\mathrm{m}^{-1}$.

Over the whole wavelength range the signal power exceeds 3 W (see Fig. 9). The idler power is about 0.6 W. The variations of the idler power are caused by the wavelength-dependent transmission of the cavity mirror M7.

The characteristic parameters of a synchronously pumped OPO, such as the output power, the pulse duration and the spectral pulse width critically depend on the cavity length. A change of the cavity length causes a change of the temporal overlap of the resonant OPO pulse and the laser pulse. The temporal overlap is also changed by the GVM between the three interacting pulses. The GVM between the pump and the signal pulse is 43 fs/mm, and the GVM between the pump and the idler pulse 280 fs/mm. In the crystal the idler pulse thus propagates faster than the signal and pump pulses. For the signal-resonant LBO OPO the interaction length is practically not limited by temporal walk-off between the pump and signal pulses since the maximum retardation of the pump pulse is only 882 fs for the 18-mm long LBO crystal. This is less than 15% of the duration of the pump pulse and can thus be neglected. For this reason the OPO operation should tolerate length detunings that are a substantial fraction of the length of the pump pulse. For $T_{OC} = 37\%$ the measured maximum length detuning (which maintains OPO operation) was 250 μm. This detuning corresponds to a delay of the signal pulse of 500 μm which is almost one quarter of the length of the pump pulse. For lower output coupling ($T_{OC} = 18\%$) the detuning is increased to 300 μm because the smaller T_{OC} lowers the OPO's threshold power.

Figure 10 shows the characteristic parameters of the OPO (such as power, pulse duration, spectral width and time–bandwidth product) as functions of the resonator length detuning ΔL. For $\Delta L = 0$ μm the delay between the pump and signal pulse is zero at the front facet of the crystal. If only the GVM of the pump and signal is considered, a maximum output power is expected for $\Delta L = 66$ μm. As the group velocity of the idler pulse is larger than that of both the pump and the signal wave, the maximum output power is shifted to a value of $\Delta L > 66$ μm. As seen in Fig. 10 the maximum output power of 3.4 W is measured for $\Delta L = 170$ μm and the OPO operates above the threshold for 120 μm $< \Delta L <$ 380 μm. This clearly indicates that the group velocity of the nonresonant wave is of relevance to the dependence of the OPO

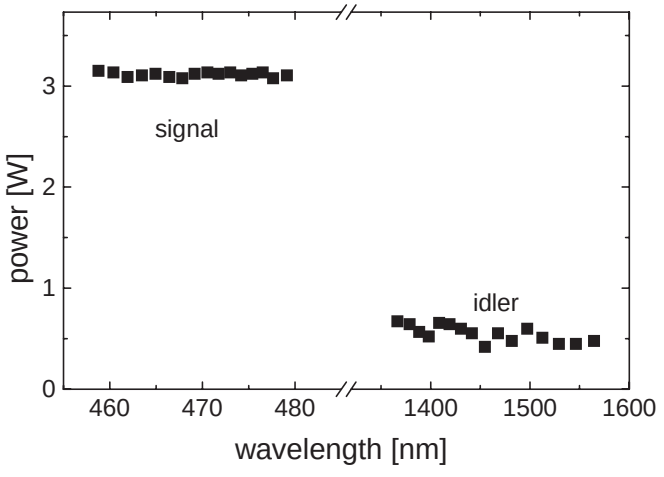

Fig. 9. Signal and idler output power as a function of the wavelength. The 355-nm pump power is 9 W, the OC transmission is 37%

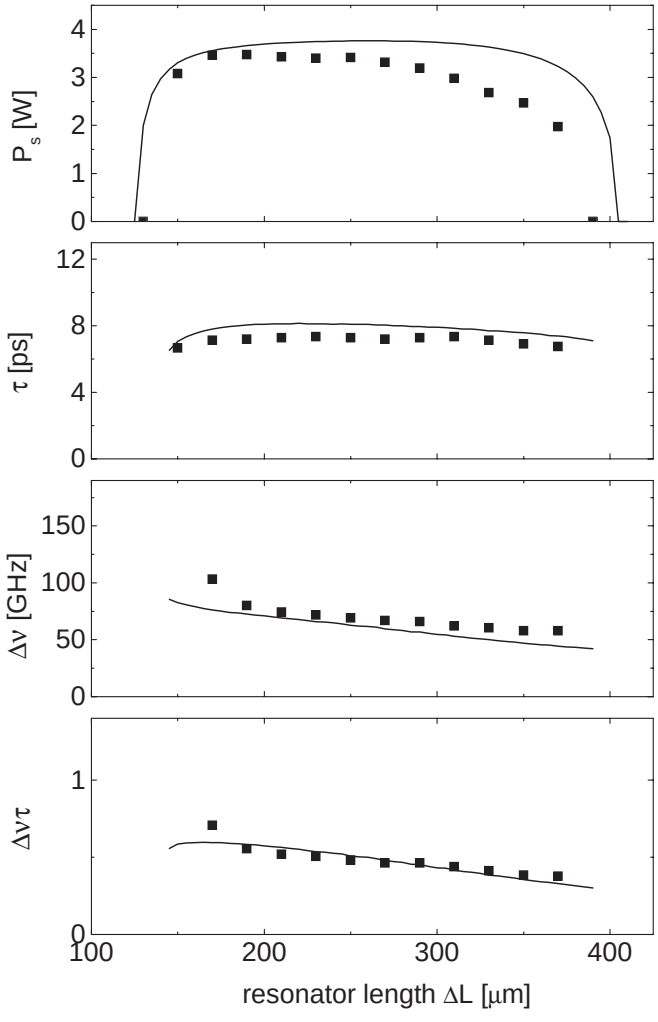

Fig. 10. Dependence of the 479-nm signal power P_s, pulse duration τ, spectral width $\Delta\nu$ and time–bandwidth product $\Delta\nu\tau$ on the resonator length. *The squares* are the measured values, *the solid lines* represent the data of the numerical analysis. The OC transmission is 37%, the 355-nm pump power is 9 W

performance on ΔL. This could be seen also from a comparison with a KTA-OPO, which was pumped by 1064-nm radiation [24]. In this OPO the GVM between the pump and the signal wave (55 fs/mm) is almost the same, the group velocity of the idler wave is, however, smaller than that of the pump and the signal wave. For that OPO, operation above the threshold was achieved only for values of $\Delta L < 100\,\mu$m, whereas the present LBO OPO operates only for $\Delta L > 100\,\mu$m.

The result of the numerical analysis, which is shown in Fig. 10 by the solid lines, is, in general, in good agreement with the measured data. A deviation is observed for the measured output power which decreases faster than predicted for detunings, $\Delta L > 240\,\mu$m. The difference between the calculated and the measured values might result in the simplification of the numerical model, which is given by the approximation of the spatial overlap of the three interacting beams by beam overlap factors. The pulse duration τ is almost independent of ΔL. In fact, for $170\,\mu\text{m} < \Delta L < 350\,\mu$m the measured pulse duration varies only in the narrow range 7–8 ps. Also, the measured small increase of the spectral pulse width $\Delta\nu$ with decreasing ΔL is confirmed by the numerical analysis. The time–bandwidth product $\Delta\nu\tau$ decreases with increasing resonator length from 0.70 to 0.33. These values indicate that the pulses are always close to the bandwidth limit.

The calculations indicated that the temporal pulse profile changes with cavity length. The pulse shape is, in general, nonsymmetric. This is of course of importance for the interpretation of the measured autocorrelation traces. Usually it is assumed that the shape of the pump pulse is a symmetrical sech^2 pulse and that the OPO reproduces the shape of the pump pulse. The evaluation factor used is thus 0.64. The calculations showed, however, that this evaluation factor changes from 0.65 to 0.81 if ΔL is changed from 170 μm to 350 μm.

The results of the numerical analysis depend critically on the pump pulse duration and the nonlinear coefficient of LBO. The pulse duration of the third harmonic was determined to be 7.5 ± 1.0 ps. The value of the nonlinear coefficient d_{31} for LBO given in the literature varies from 0.67 to 1.1 pm/V [26–28]. The calculated results (power, pulse duration and spectral width of the OPO pulses as functions of the resonator length, and output power and pulse duration as functions of the OC transmission) are in good agreement with the experimental data for a pump pulse duration of 7 ps and a nonlinear coefficient of 0.55 pm/V. For longer pump pulses (8 or 9 ps) the change of the above-mentioned parameters with resonator length does not match the results of the numerical analysis. For other values of the nonlinear coefficients (e.g. 0.4 pm/V or 0.7 pm/V) the calculated optimum OC transmission did not agree with the experimental value.

Because the efficiency of the OPO is larger than 70% the pump pulse should be strongly depleted. In addition, part of the OPO radiation should be reconverted. These effects influence the temporal profile of the transmitted pump pulse, which was investigated using a cross-correlation measurement with the green pulse, using difference-frequency mixing (DFM). For different resonator lengths a symmetry change of the cross-correlation signal is expected, because the resonant signal pulse is delayed in the cavity and depletes the pump pulse nonsymmetrically. Figure 11 shows measured and calculated cross-correlations of the transmitted pump wave for different resonator lengths ($\Delta L = 120\,\mu$m, 200 μm, 240 μm and 280 μm). In this diagram the front part of the pulse is on the right side and the rear part is on the left side. For $\Delta L = 120\,\mu$m (Fig. 11a) the transmitted pump pulse is not changed because the OPO is below the threshold. For $\Delta L = 200\,\mu$m (Fig. 11b) the pump pulse is depleted at the rear part, which results in a nonsymmetric cross-correlation. For $\Delta L = 240\,\mu$m (Fig. 11c) the cross-correlation is nearly symmetric and is broadened. The pump pulse power is depleted but partly reconverted in its center. For $\Delta L = 280\,\mu$m (Fig. 11d) the symmetry of the cross-correlation changed such that the pump pulse was depleted in the front part.

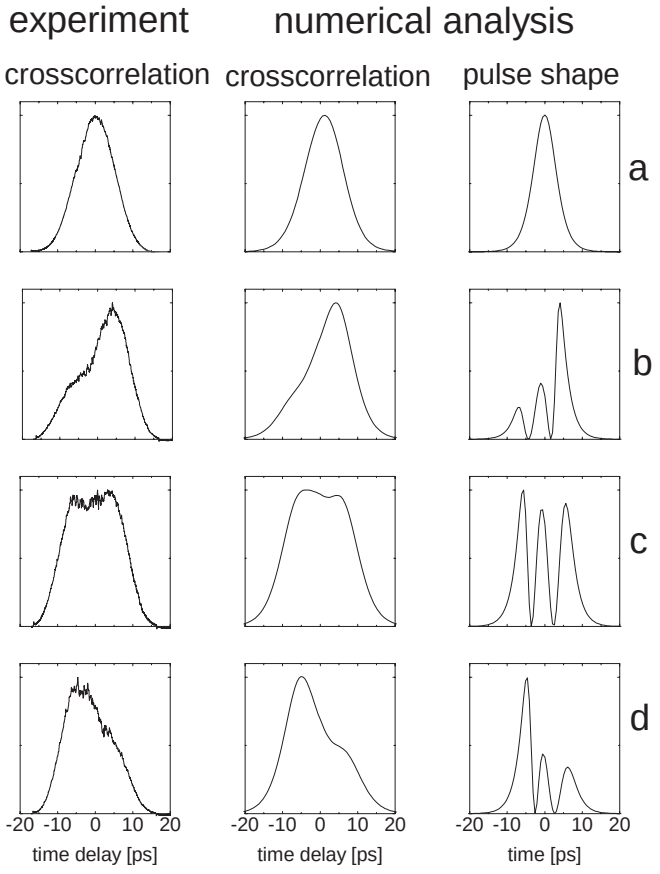

Fig. 11. Cross-correlation traces of the pump pulses transmitted by the LBO OPO cavity for resonator length detunings $\Delta L = 120\,\mu$m (**a**), 200 μm (**b**), 240 μm (**c**) and 280 μm (**d**) as measured in the experiment and calculated by the numerical simulation. Also shown are the calculated temporal pulse shapes. The wavelength of the signal wave is 479 nm, the OC transmission is 37%, the 355-nm pump power is 9 W

Because of the good agreement between the calculated and the measured cross-correlation traces we assume that the numerically calculated temporal pulse profiles of the transmitted pump give a good indication of the real shape of the experimental pulse profiles.

In the LBO OPO described so far the LBO crystal was Brewster-cut. This minimizes the resonator internal losses for the resonant signal radiation but causes losses of about 17% for the pump beam. This loss can be reduced using a LBO crystal with plane facets which are AR-coated for the resonant signal wave. It should be noted that this crystal causes no astigmatism in the OPO cavity. In addition, the adjustment of

the cavity is easier because the pump and the resonant signal beam are collinear.

Because the AR-coatings showed a lower damage threshold for the UV pump radiation at elevated crystal temperatures this OPO was operated only at room temperature. The wavelengths of the generated signal and idler wave were 479 nm and 1371 nm, respectively. The OPO crystal with a length of 20 mm was cut for noncritical phasematching ($\Theta = 0°$). The crystal was AR-coated for the signal wave ($R < 0.5\%$) and highly transmissive for the pump and idler waves. Because of the reduced losses for the pump radiation the OPO generated more than 4.2 W of blue 479-nm radiation. The optimum T_{OC} was 50%. It is interesting to note that due to the high gain the OPO could be operated even with an OC transmission of 92% (uncoated SF57 glass substrate). The power of the 1.371-μm idler wave was 1.2 W. In conclusion, the LBO OPO with AR-coated crystal provides a higher signal and idler output compared to the OPO operated with a Brewster-cut LBO crystal. The tunability is limited, however, to about 5 nm, due to the temperature sensitivity of the damage threshold of the AR crystal coatings.

3 Idler-resonant LBO OPOs

3.1 Noncritically phasematched idler-resonant OPO using a Brewster-cut crystal

As shown by the results discussed so far the 355-nm pumped signal-resonant LBO OPOs are high-power light sources tunable in the blue spectral range. If, however, the IR idler wave should be used to generate laser light in the red spectral range using SFM of the 1.535-μm idler wave with the 1.064-μm laser radiation, it is advantageous to operate the OPO with an idler-resonant cavity. In this way the intracavity losses of the e-polarized idler wave could be minimized, and the reflection losses for the e-polarized pump at the Brewster facet are negligible. Only the nonresonant o-polarized signal wave experiences reflection losses at the Brewster facet and transmission losses at mirror M7.

The experimental setup of the idler-resonant noncritically phasematched OPO operated with a Brewster-cut crystal is similar to that of the signal-resonant OPO (shown in Fig. 1) except that the mirrors are highly reflective at 1.5 μm. The 18-mm long LBO crystal is Brewster-cut for the resonant e-polarized idler wave. An oven is used to control and vary the crystal temperature for wavelength tuning. Because both the pump and the resonant idler wave are e-polarized the pump light enters the crystal with low losses at the Brewster facet. The transmission losses at lens L6 and mirror M6 are 13%. These losses reduce the laser power from 9.0 W (in front of L6) to 7.8 W inside the crystal. Compared to the signal-resonant OPO the crystal-internal peak pump power is thus higher by 18%, which should provide a somewhat higher parametric gain. In fact, a pump depletion of more than 70% was measured for OC transmissions in the range 12%–41% if mirrors (M6 and M7) with a radius of curvature of $r = -200$ mm were used. For a curvature of $r = -150$ mm a pump depletion of 70% was measured for OC transmissions as high as 49%. The smaller radius of curvature reduces the waist of the resonator mode from 60 μm ($r = -200$ mm) to 43 μm ($r = -150$ mm). A further reduction of the mode diameter to 28 μm (using mirrors with $r = -100$ mm) reduced, however, the efficiency of the OPO. In this case the beam waists of the resonator mode and of the focused pump beam are almost equal, but the confocal parameters of both beams are different by a factor of 4.3 due to the different wavelengths of the 355-nm pump and the 1.535-μm idler wave.

With the highest pump depletion of 75% the measured power of the resonant idler wave is 1.2 W. This is about twice the value of the idler power obtained with the signal-resonant OPO with Brewster-cut crystal facets. The power of the blue-signal radiation was 3.1 W. This corresponds to a conversion efficiency of 75% when the losses at the Brewster facet, at M7 and L7, are taken into account. These losses amount to a total loss of 35%. Despite the higher pump peak power the performance of the OPO is thus (in comparison to the signal-resonant OPO) not improved by a considerable amount.

As observed for the signal-resonant OPO the efficiency of the idler-resonant OPO depends on the resonator length, which influences the temporal overlap of the pump, signal and idler pulses inside the crystal. For the signal-resonant OPO the maximum output was achieved for $\Delta L = 140$ μm, close to the lower limit of the possible length detuning range and – as seen from Fig. 10 – the OPO operated above the threshold for 120 μm $< \Delta L <$ 380 μm. The OC transmission used in these measurements was 37%. If the idler-resonant OPO is operated with the same OC transmission the resonator length can be changed in the range 520 μm $< \Delta L <$ 780 μm and (in contrast to the signal resonant OPO) the maximum output power is achieved for $\Delta L = 735$ μm, which corresponds to the upper limit of the length detuning range.

A numerical analysis indicated that for the given pump intensity the signal-resonant OPO should provide a maximum efficiency of 81% ($\Delta L = 235$ μm), whereas for the idler-resonant OPO the efficiency should be 78% ($\Delta L = 730$ μm). The numerical analysis also indicated that the threshold of the signal-resonant OPO should be 1.82 W for $T_{OC} = 40\%$ and an optimized cavity length ($\Delta L = 180$ μm). For the idler-resonant OPO the corresponding values are 1.88 W and $\Delta L = 730$ μm. It should be noted that for the idler-resonant OPO the calculations provide the same value for the cavity lengths which are required for the lowest threshold and the maximum efficiency. This is not the case for the signal-resonant OPO, where these resonator lengths differ by 55 μm (if $T_{OC} = 40\%$). The reasons for the different behavior are the GVM between the pump and the resonant wave and the pump depletion. For the idler-resonant OPO the GVM is 281 fs/mm which is 5.7 times larger than in the signal-resonant OPO.

Wavelength tuning of the idler-resonant OPO was achieved by heating the LBO crystal. The tuning range was limited to 1450–1600 nm by the wavelength dependence of the reflectivity of the used mirror set. The corresponding tuning of the signal wave was 470–457 nm.

The measured pulse duration was typically 7 ps for an OC transmission of 30% and was independent of the resonator length within 90% of the length detuning range. The width of the measured pulse spectrum was 61 GHz. The corresponding time–bandwidth product of 0.43 indicates that the pulses are almost bandwidth limited.

3.2 Critically phasematched OPOs

Whereas in NCPM OPO the crystal has to be heated to 163 °C to generate an idler wave of 1535 nm, critical phasematching allows the generation of 1535-nm idler radiation at room temperature. The characteristic parameters of the LBO crystals required for NCPM and CPM are compared in Table 3. To generate a wavelength of 1535 nm at room temperature the critical phasematching angle is $\Theta = 14.6°$. Thus, spatial walk-off, which is zero for NCPM, increases with respect to the signal wave to 0.8° for the pump and 0.7° for the idler wave. Both beams are e-polarized waves. The difference between the walk-off of the resonant idler and the pump wave is only 0.1°. Since the pump and the resonant idler wave propagate almost collinearly no significant reduction of the gain is expected by using CPM. Also, the spectral acceptance as well as the GVM differ by less than 5%. However, a decisive influence on the gain is expected from the angular acceptance, which is reduced for CPM by two orders of magnitude. This could also have an influence on the spatial profile of the generated OPO waves.

In the experiment the CPM crystal had the same dimensions as the NCPM crystal. Thus, the OPO resonator could be aligned with the pump radiation and the NCPM crystal. After inserting the CPM crystal parametric oscillation could be started easily by tilting the end mirror in the walk-off direction. The OPO performance was optimized by walking the beam within the resonator by successively misaligning and realigning the end mirrors.

This critically phasematched OPO converted 89% of the pump inside the crystal into signal and idler radiation. This conversion efficiency was determined from the measured pump depletion. In these measurements the OC was replaced by a HR mirror. Since the idler transmission of each cavity mirror is below 0.2% the overall transmission of the folded resonator is less than 2%. The power of the generated signal wave was 3.4 W. Due to the various losses in the resonator the external signal power corresponds to 5.2 W generated inside the crystal. The parametric gain of this OPO, however, is considerably smaller compared to the NCPM OPO. This is clearly indicated by a maximum OC transmission of 33% compared to 68% for the NCPM OPO.

In the experiments described so far a CPM-LBO crystal with Brewster-cut facets was used. For comparison this crystal was replaced by an AR-coated CPM-LBO crystal.

Figure 12 shows the signal and idler output power as functions of the OC transmission of the CPM idler-resonant OPO with an AR-coated crystal at room temperature. As expected, the power of the nonresonant signal wave increases for lower OC transmissions. The highest signal power is in fact obtained with a HR mirror as the end mirror. In this case the generated signal power is 5.0 W which corresponds to a crystal internal conversion efficiency of 85%.

Because of the lower parametric gain the threshold power of the CPM OPO should be higher than the threshold of the NCPM OPO. Figure 13 compares the pump power at the threshold for the NCPM signal-resonant and the CPM idler-resonant OPO as functions of the OC transmission. The threshold of the CPM OPO is more than three times higher

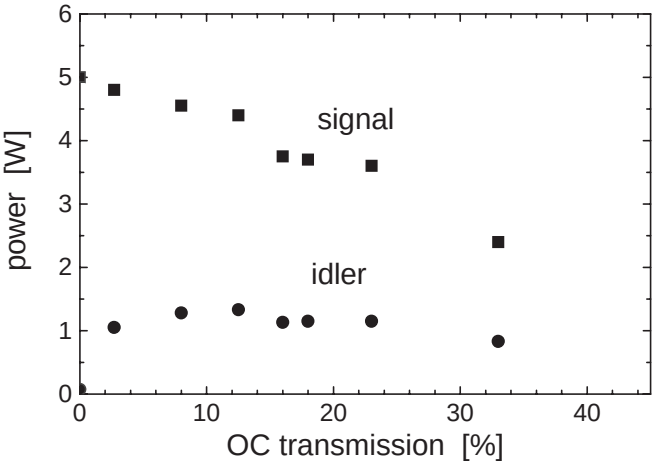

Fig. 12. Average power of the 462-nm signal and the 1535-nm idler wave of the idler-resonant CPM OPO measured as a function of the OC transmission. The OPO is operated with an AR-coated LBO crystal at room temperature

Table 3. Characteristic crystal parameters of LBO used in the 355-nm pumped OPOs with noncritical (NCPM) or critical (CPM) phasematching and an idler wavelength of 1535 nm. The data are calculated with the Sellmeier equations given in [19, 21]

		NCPM [21]	CPM [19]
Phasematching		Type II e-oe, $\Theta = 0°$, z-cut	Type II e-oe, $\Theta = 14.6°$, xz-plane
Nonlinearity [28]	d_{eff}	−1.1 pm/V	−1.0 pm/V
Spatial walk-off	ϱ		
Pump		0	−0.8°
Idler		0	−0.7°
Bandwidth acceptance	$\Delta\lambda \cdot L$		
Signal		0.26 nm · cm	0.26 nm · cm
Idler		2.9 nm · cm	2.9 nm · cm
Angular acceptance		$\Delta\theta \cdot \sqrt{L} = 216$ mrad · $\sqrt{\text{cm}}$	$\Delta\theta \cdot L = 1.8$ mrad · cm
Group velocity mismatch			
Pump/signal		43 fs/mm	43 fs/mm
Pump/idler		280 fs/mm	280 fs/mm

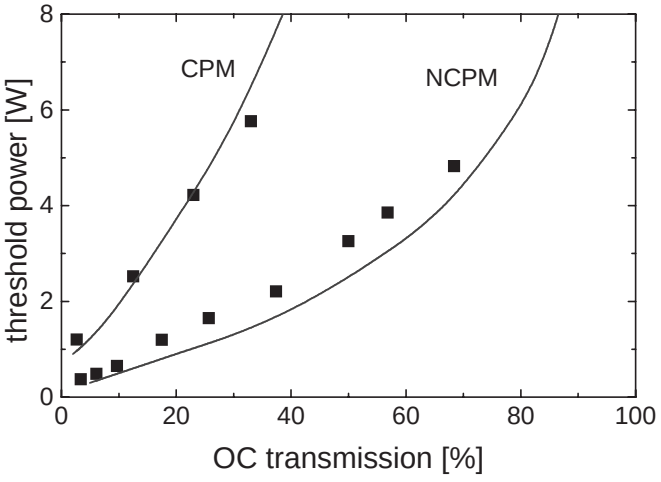

Fig. 13. Pump power at the threshold as a function of the OC transmission for the signal-resonant NCPM and the idler-resonant CPM OPO. *The squares* represent the measured data, *the solid line* the values obtained by the numerical analysis

than that of the NCPM LBO OPO. The solid lines, which represent the values obtained from the numerical analysis are in rather good agreement with the experimental data.

The numerical calculations show that the spatial walk-off also influences the optimum overall phase mismatch. For the same focusing conditions of the pump radiation (waist: 30 μm) the optimum phase mismatch is $\Delta k = -110\,\mathrm{m}^{-1}$ for the CPM OPO compared to $\Delta k = 140\,\mathrm{m}^{-1}$ for both the noncritically phasematched signal- and idler-resonant OPO. These values indicate that in the CPM OPOs the walk-off strongly changes the relative phases of the three interacting waves.

4 Comparison of the performance of the NCPM and CPM LBO OPO

The investigated OPOs are either signal- or idler-resonant. They also differ in the phasematching (NCPM or CPM) and in the facet geometry of the nonlinear crystal (Brewster-cut or flat AR-coated). The performance of the different OPOs are compared in Table 4 with respect to the output power, optimum OC transmissions and beam quality. The choice of the crystal geometry and which wave is resonated mainly influences the losses in the OPO. In particular, for the resonant wave the losses have to be minimized, whereas the nonresonant wave could experience larger losses (due, for example, to reflections at the Brewster facets or the low transmission of the cavity mirrors).

With the signal-resonant NCPM OPOs the highest blue output of 4.3 W was obtained with an OPO operated with an AR-coated crystal pumped by 9 W of 355-nm radiation. In addition to the high signal output the idler output was as high as 1.2 W, since in this configuration the idler losses are lower compared to an OPO with a Brewster-cut crystal. Also, the values of the optimum conversion efficiency (78%) and the corresponding OC transmission (50%) are higher compared to those of OPOs with a Brewster-cut crystal. However, for widely tunable operation in the blue spectral range the signal-resonant LBO OPO with Brewster-cut crystal is preferred as long as durable, high-temperature- and high-power-resistant AR-coatings are not available.

The highest blue output of 5 W is obtained with an idler-resonant CPM OPO. This OPO uses a crystal with flat AR-coated facets and is operated at room temperature. An interesting feature is the very high internal efficiency of this CPM OPO of 85% which is achieved with a HR end mirror. This limits the output power of the resonant wave to less than 0.07 W. It should be noted that with an OC transmission of 12% the output of the resonant idler wave is 1.3 W. The total OPO output of the resonant and nonresonant waves decrease, however, to 5.7 W, but the internal conversion efficiency (indicated by the measured pump depletion) is still as high as 75%. The efficiency is thus fully comparable to the internal conversion efficiencies obtained with the NCPM (signal- or idler-resonant) LBO OPOs.

An important property of the OPO is the spatial quality of the generated beams. For most applications an M^2 value of less than 1.2 is desired. Table 4 shows that the resonant beam is always diffraction limited with M^2 values of less than 1.1 regardless of whether the OPO is noncritically or critically phasematched. This is because the resonator determines the intensity distribution in the beam, and the spatial walk-off or a limited angular acceptance are of minor influence. On the other hand the spatial quality of the nonresonant beam depends critically on the phasematching conditions. For noncritically phasematched LBO OPOs the M^2 value of the nonresonant wave is always less than 1.2, such that in general the noncritically phasematched OPOs provide a high beam quality for both the idler and signal beams. For critically phasematched OPOs the M^2 value of the nonresonant wave is as high as 2.0 (for an OPO with a Brewster-cut crystal) and even 3.0 for an OPO using an AR-coated crystal. The M^2 values are measured for a resonator length that provides an optimum conversion efficiency.

5 Generation of red 629-nm radiation

SFM of the generated 1535-nm OPO idler wave and of the residual 1064-nm laser radiation is a convenient way to generate powerful red 629-nm radiation. For this SFM process potassiumtitanylarsenate (KTA) is appropriate, because of its high nonlinearity ($d_{\mathrm{eff}} = 4.2\,\mathrm{pm/V}$ [31]). Type-II phasematching is achieved for $\phi = 90°$ and $\Theta = 33°$. Because of the small spatial walk-off of 0.1° the phasematching is almost noncritical. The setup of the SFM experiment is similar to the arrangement used for TH generation. A telescope adapts the 1064-nm laser beam in diameter and divergence to the 1535-nm idler radiation. Both beams are superimposed collinearly and focused with a spherical lens ($f = 100\,\mathrm{mm}$) into the 15-mm long AR-coated KTA crystal. With an optical delay line for the 1535-nm pulses the temporal overlap of the two pulses is optimized.

In the SFM we used the 1064-nm laser beam transmitted by mirror M3 (Fig. 1). The power of this beam is up to 6.4 W. An autocorrelation of the pulses showed no distortions of the temporal pulse shape. The pulse width was 16 ps.

Table 4. Comparison of the performance of the investigated OPOs. For further details see the text

Resonant wave		Phasematching		Crystal facets		λ_{sig} (nm)	λ_{idl} (nm)	P_{sig} (W)	P_{idl} (W)	η (%)	T_{oc} (%)	M^2_{sig}	M^2_{idl}
Signal	Idler	NCPM	CPM	Flat AR	Brewster								
●		●			●	479	1371	3.4	0.65	75	37	< 1.1	< 1.2
●		●		●		479	1371	4.3	1.2	78	50	< 1.1	< 1.2
	●	●			●	470	1451	3.1	1.2	75	33	< 1.2	< 1.1
	●		●		●	462	1535	3.4	0.05	89	0 (HR)	< 2.0	< 1.1
	●		●	●		462	1535	5.0	0.07	85	0 (HR)	< 3.3	< 1.1

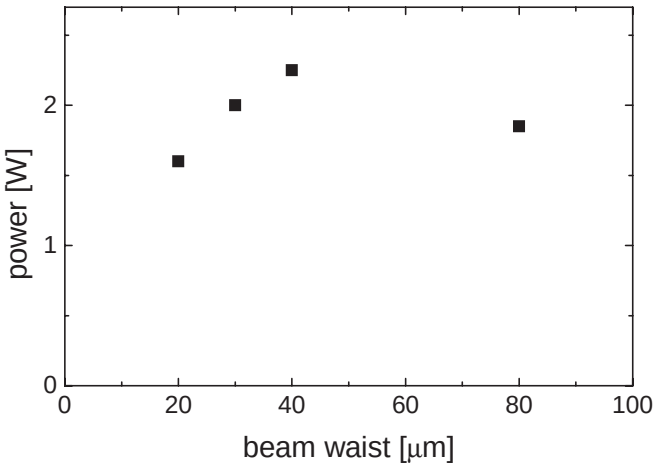

Fig. 14. Power of the 629-nm SFM radiation as a function of the beam waists of the 1.5-μm idler and the 1.064-μm laser beam

A measurement of the beam quality provided an M^2 value of less than 1.4.

Using a power of 1.535-μm radiation of 1.25 W (generated by the NCPM signal-resonant OPO with AR-coated crystal) and a 1.064-μm laser power of 5.7 W the SFM generated red 629-nm radiation with a power of up to 2.25 W. Figure 14 shows the dependence of the obtained power on the beam waists of the two input beams. As seen from this figure, 2.25 W of 629-nm light is generated if the waist of the two beams is 40 μm. The red output power corresponds to a conversion efficiency of 32%. In this case 74% of the idler power is converted into red radiation. Even a change of the temporal overlap of the input pulses by 8 ps did not change the conversion efficiency significantly, which indicates that the nonlinear conversion is highly saturated.

Besides the signal-resonant NCPM OPO, both the critically phasematched as well as the noncritically phasematched idler-resonant OPOs are useful for generation of red laser light. However, the spatial beam quality of the nonresonant 462-nm wave of the critically phasematched OPO is low. Thus, only the noncritically phasematched OPOs provide simultaneously red and blue radiation in a beam of high spatial quality.

As a result, 4.3 W of blue 479-nm signal radiation and 2.25 W of red 629-nm light (generated by SFM of the 1.535-μm idler wave and 1.064-μm laser radiation) are obtained with the signal-resonant NCPM LBO OPO (AR-coated, flat facet crystal). With respect to the 28 W of 1064-nm pump laser power, the total visible output of 6.5 W corresponds to an overall conversion efficiency of almost 23%.

6 Summary

The third-harmonic generation of the 28-W output of a mode-locked cw diode-pumped Nd:YVO_4 oscillator–amplifier system in a type-II phasematched LBO crystal generates 9.0 W of mode-locked 355-nm pulses in a nearly diffraction-limited beam ($M^2 < 1.3$). The pulse duration is 7.5 ps, the repetition rate is 84 MHz. The 355-nm UV radiation is used to synchronously excite different LBO OPOs.

The OPOs investigated include a NCPM signal-resonant OPO with a Brewster-cut LBO crystal which generated more than 3.0 W of blue signal wave output. This output corresponds to an OPO conversion efficiency of 70%. The wavelength of the blue radiation is tunable in the range 457–479 nm by changing the crystal temperature in the range 20–190 °C. The results of detailed experimental investigations (which include, for example, the dependence of the output power and pulse duration on the resonator properties such as OC transmission or cavity length) are in good agreement with the predictions of a numerical analysis based on Gaussian laser and OPO beams. Besides the signal-resonant OPO idler-resonant OPOs are investigated. A NCPM idler-resonant LBO OPO generated more than 1.2 W of output power tunable in the infrared region (1450–1600 nm). Sum-frequency mixing of idler pulses at 1.535 μm and the 1.064-μm laser radiation generated 2.25 W of red light at 629 nm. The performance of the idler-resonant NCPM OPOs is compared with CPM idler-resonant OPOs. Although these OPOs show a higher threshold they provide total internal conversion efficiencies as high as 89%. The highest output in the blue spectral range of 5.0 W at 462 nm was thus generated using a CPM idler-resonant OPO.

In conclusion we investigated experimentally and numerically the performance of high-power synchronously pumped LBO OPOs in different configurations (with respect to the resonant wave, the phasematching and the crystal geometry). The results demonstrate that these all-solid-state sources should be well suited for many applications.

References

1. P.F. Curley, A.I. Ferguson: Opt. Commun. **80**, 365 (1991)
2. R.J. Ellingson, C.L. Tang: Opt. Lett. **17**, 343 (1992)
3. A. Nebel, R. Beigang: Opt. Lett. **16**, 1729 (1991)
4. M. Watanabe, R. Ohmukai, K. Hayasaka, H. Imajo, S. Urabe: Opt. Lett. **19**, 637 (1994)
5. P.E. Powers, R.J. Ellingson, W.S. Pelouch, C.L. Tang: J. Opt. Soc. Am. B **10**, 2162 (1993)
6. R.J. Ellingson, C.L. Tang: Opt. Lett. **18**, 438 (1993)
7. A. Nebel, H. Frost, R. Beigang, R. Wallenstein: Appl. Phys. B **60**, 453 (1995)
8. D.T. Reid, M. Ebrahimzadeh, W. Sibbett: J. Opt. Soc. Am. B **12**, 1157 (1995)
9. S. French, M. Ebrahimzadeh, A. Miller: Opt. Commun. **128**, 166 (1996)
10. S. French, M. Ebrahimzadeh, A. Miller: Opt. Lett. **21**, 976 (1996)
11. Z.G. Lü, G.C. Cho, G. Lüpke, H. Kurz: Opt. Commun. **133**, 263 (1997)
12. T.J. Driscoll, G.M. Gale, F. Hache: Opt. Commun. **110**, 638 (1994)
13. J.D. Kafka, M.L. Watts, J.W. Pieterse: J. Opt. Soc. Am. B **12**, 2147 (1995)
14. A. Agnesi, C. Pennacchio, G.C. Reali, V. Kubecek: Opt. Lett. **22**, 1645 (1997)
15. D. Wang, C. Grässer, R. Beigang, R. Wallenstein: Opt. Commun. **138**, 87 (1997)
16. M.J. McCarthy, S.D. Butterworth, D.C. Hanna: Opt. Commun. **102**, 297 (1993)
17. A. Robertson, A.I. Ferguson: Opt. Lett. **19**, 117 (1994)
18. S.D. Butterworth, S. Girard, D.C. Hanna: J. Opt. Soc. Am. B **12**, 2158 (1995)
19. B. Wu, F. Xie, C. Chen, D. Deng, Z. Xu: Opt. Commun. **88**, 451 (1992)
20. J.Y. Huang, Y.R. Shen, C. Chen, B. Wu: Appl. Phys. Lett. **58**, 1579 (1991)
21. K. Kato: IEEE J. Quantum Electron. **QE-30**, 2950 (1994)
22. E.C. Cheung, J.M. Liu: J. Opt. Soc. Am. B **8**, 1491 (1991)
23. C. Fallnich, B. Ruffing, T. Herrmann, A. Nebel, R. Beigang, R. Wallenstein: Appl. Phys. B **60**, 427 (1995)

24. B. Ruffing, A. Nebel, R. Wallenstein: Appl. Phys. B **67**, 537 (1998)
25. G.D. Boyd, D.A. Kleinman: J. Appl. Phys. **39**, 3597 (1968)
26. S.P. Velsko, M. Webb, L. Davis, C. Huang: IEEE J. Quantum Electron. **QE-27**, 2182 (1991)
27. S. Lin, Z. Sun, B. Wu, C. Chen: J. Appl. Phys. **67**, 634 (1990)
28. D.A. Roberts: IEEE J. Quantum Electron. **QE-28**, 2057 (1992)
29. M. Okada, S. Ieiri: IEEE J. Quantum Electron. **QE-7**, 560 (1971)
30. J.M. Liu, G. Zhou, S.J. Pyo: J. Opt. Soc. Am. B **12**, 2274 (1995)
31. L.K. Cheng, L.-T. Cheng, J.D. Bierlein, F.C. Zumsteg, A.A. Ballmann: Appl. Phys. Lett. **62**, 346 (1993)